Mineralization Kinetics of Hydroxyapatite/Chitosan Composite in a Simulated Body Fluid

Liping Zeng[1], Deliang He [1] and Xianglong Liu [2]
1 Department of Building Engineering, Hunan Institute of Engineering, Xiangtan, Hunan 411104,China
2 College of Chemistry and Chemical Engineering, Hunan University, Changsha, 410082, PR China

Keywords: Hydroxyapatite; Chitosan; Mineralization; Electrochemical impedance spectroscopy

Abstract: This study offers provide real time and multidimensional information to the monitoring of biomaterial mineralization process. In order to investigate on real time the mineralization process of hydroxyapatite/chitosan (HAP/CS) composite in a simulated body fluid, the piezoelectric quartz crystal impedance (PQCI) technique and electrochemical impedance spectroscopy (EIS) was used to reveal the mineralization kinetics processes for bone tissue engineering. Various characterization techniques were analyzed by Fourier transformed infrared (FT-IR), X-ray diffraction (XRD) and scanning electrode microscopy (SEM). A decrease of the frequency (f) and an increase of the charge transfer resistance (R_{ct}) at the gold electrode/solution interface were observed due to the mineralization of HAP/CS composite. According to the data of the frequency and static capacity (C_s), the correlative kinetic equations and parameters were obtained by nonlinear regression. The results show that the mineralization process of HAP/CS is divided into two stages: the nucleation stage and the crystal growth stage, which paves the way for applications of bone tissue engineering.

1 INTRODUCTION

Calcium phosphates that have a similar chemical composite with the mineral phase of natural bone are excellent candidates for bone repair and have been used in bone tissue engineering for two decades(Baker et al., 2006;Shadanbaz et al., 2012; Chen et al., 2014). Hydroxyapatite ($Ca_{10}(PO_4)_6(OH)_2$, (HAP) is one of the most important and most widely used among calcium phosphate bioceramics because of its excellent osteoconductivity and bone replacement abilities(Liu et al., 2015; Cengiz et al., 2008; Balasundaram et al., 2006; Wang et al., 2007. However, HAP use for reconstruction of a load bearing bone is limited by its brittleness. To improve the use of the HAP, hydroxyapatite/chitosan (HAP/CS) composite polymer-ceramic has been proposed and widely investigated (Petro et al., 2016; Pangon et al., 2016; Zhao et al., 2011). In recent years, significant research effort has been developed for preparation and characterization of HAP/CS for bone tissue engineering(Jiang et al., 2008; Zhang et al., 2012). HAP/CS nanocomposite rods have been prepared by in situ hybridization, and their mechanical properties of bending and compressive strength properties are enhanced(Bayrak etal., 2017; Lei et al., 2017). HAP/CS composite in-vitro investigations of biological mineralization are very useful for correctly simulating in vivo conditions, since the assays allow investigators not only to predict the behavior of bioactive implant biomaterial in the body but also to understand the physical-chemical background of mineralization. One of the most important characteristics of these bioactive artificial bone materials is that there is bone-like carbonate apatite, which is chemically and structurally equivalent to the mineral phase in bone and provides an interfacial bonding between materials and tissues. This apatite layer can be formed during mineralization process in a simulated body fluid (SBF) solution(Ohtsuki et al., 2010; Shahriarapanah et al., 2016; Li et al., 2010). Manjubala et al. reported the mineralization process of nano-hydroxyapatite-chitosan by double diffusion technique and analyzed the phase purity of apatite using X-ray diffraction (XRD) and Fourier transformed infrared (FT-IR) analysis(Manjubala et al., 2006; Meng et al., 2015). Furthermore, several studies have made efforts to accelerate the

mineralization process using modified simulated body fluid(Kong et al., 2006; Ying et al., 2011; Barrere et al., 2002). The traditional mineralization evaluation is mainly based on static characterization by XRD, FT-IR and scanning electrode microscopy (SEM). Few real-time kinetic investigations have been reported in the literatures. The piezoelectric quartz crystal impedance (PQCI) technique is a useful tool not just for providing multidimensional information reflecting some physical and chemical properties of the investigated system (Muramatsu et al., 1990; Zeng et al., 2009; Sauerbrey et al.,1959), but also for on-line monitoring the mineralization process of HAP/CS composite in a SBF solution.

This work focuses on the kinetic process of mineralization of HAP/CS composite in a SBF solution. In addition to PQCI that helped analyze the kinetic process and mechanism, the cyclic voltammetry (CV) and electrochemical impedance spectroscopy (EIS) were used to characterize film surface. Furthermore, to obtain a comprehensive understanding of the nucleation and growth of HAP, the crystal structure and morphology were examined by FT-IR and SEM.

2 MATERIALS AND METHODS

2.1 Materials

CS (molecular weight 2.0×10^5) was supplied by the Sigma Company, and the degree of deacetylation and purity of CS are 89% and 98%, respectively. AT-cut 8MHz piezoelectric quartz crystal (PQC) of approximately 15 mm diameter with gold electrodes (8 mm in diameter) was obtained from 704 Company (Beijing China). Calcium nitrate [$Ca(NO_3)_2{\cdot}4H_2O$], diammonium hydrogen phosphate [$(NH_4)_2HPO_4$], ammonia[$NH_3{\cdot}H_2O$], tris(hydroxymethyl)aminomethane [$C_4H_{11}NO_3$], 2-mercaptoacetic acid [$SHCH_2COOH$], and all the inorganic salts for SBF solution and phosphate-buffered saline (PBS) were obtained from Shanghai Chemical Reagents (Shanghai, China). All the solutions were prepared with deionized water.

2.2 Preparation of HAP/CS Composite

CS was dissolved in a 1% acetic acid aqueous solution until a 1% (wt %) CS solution was obtained. Nano-HAP particles were prepared as previously described(Wang et al., 2004). Briefly, precipitate was performed by the slow addition of a 0.5 M ammonium phosphate water solution into a 0.5 M calcium nitrate anhydrous ethanol solution with stirring at room temperature. The pH value of the solution was adjusted to 11 by $NH_3{\cdot}H_2O$. After the addition of ammonium phosphate ended, the reactants were stirred for another 2 h, and then the suspension was left to settle for 24 h. The precipitate was washed with deionized water and finally with ethanol. According to our previous work(Xu et al., 2009), HAP/CS composite with mass ratio of (6/4) can be mineralizated well in SBF solution. In this experiment, HAP was dissolved into CS of acetic acid aqueous solution based on this ratio and ultrasonic dissolution for 30 min. Then the prepared HAP/CS composite solutions were kept in a refrigerator.

2.3 Preparation of SBF Solution

The SBF solution was prepared by dissolving NaCl, $NaHCO_3$, KCl, $K_2HPO_4{\cdot}3H_2O$, $MgCl_2{\cdot}6H_2O$ $CaCl_2$, and Na_2SO_4 into deionized water. The SBF solution was adjusted to physiological pH (pH 7.4) with tris-HCl buffer. The SBF concentrations were 142.5 mM Na^+, 2.6mM Ca^{2+}, 1.5mM Mg^{2+}, 5mM K^+, 147.8mM Cl^-, 1.0mM HPO_4^{2-}, 4.25mM HCO_3^- and 0.5mM SO_4^{2-}.

2.4 Preparation of PQC Sensor

In order to remove possible contamination, each of the gold electrodes of PQC was cleaned in fresh piranha solution (70% H_2SO_4, 30%H_2O_2) followed by rinsing with deionized water. Then, self-assembled monolayer was formed on the gold electrode surface by immersing it into a solution of 0.01 M 2-mercaptoacetic acid for 12 h. Subsequently, the HAP/CS composite was dropped on the surface of gold electrode of PQC by a micro-syringe. The electrode was put into an air oven to be dried at 60 ℃ for 24 h in order to remove all the acetic acid and water, and then a rigid film was obtained.

2.5 PQCI Measurement

The mineralization process of HAP/CS composite was monitored on-line using a piezoelectric impedance analyzer (HP4192 LF, America). The PQC sensor with modified (HAP/CS) electrode was dipped in SBF solution at 37±0.5 ℃. A user's program was developed using Visual Basic (VB) 5.0 to control the piezoelectric impedance analyzer, which measures the resonant frequency (*f*) of the PQCI simultaneously, and also fits the values of the

Butterworth-van Dyke (BVD) equivalent circuit parameters by Gauss-Newton nonlinear least-squares. In this work, the BVD equivalent circuit parameters were obtained in 30 s intervals, including motional resistance (R_m), motional inductance (L_m), static capacitance (C_s) and motional capacity (C_m).

2.6 Electrochemical Measurements

The mineralization properties of the HAP/CS composite were studied by electrochemical methods using EIS and CV (CHI660B electrochemical workstation, Instruments China CH). A conventional three-electrode cell was utilized: a modified electrode served as the working electrode, a platinum plate served as the counter electrode, and a saturated KCl calomel electrode served as the reference electrode. All experiments were performed at 37±0.5 ℃.

The variation of morphology and composition for the corresponding stages of mineralization products were characterized by FT-IR (Nicolet 5700, Thermo), scanning electron microscopy (SEM, JSM-6700F, Japan) and XRD (CO.. Ltd., Japan).

3 RESULTS AND DISCUSSION

3.1 PQCI Studies of Mineralization of the HAP/CS Composite in SBF Solution

The PQCI analysis technique is usually used to study the on-line interface properties of surface-modified electrodes. In piezoelectric analysis, the frequency response change (Δf) of the sensor in liquid depends on the mass and viscoelasticity changes of the sensor surface, and the change in the viscosity and density of the solution. Motional resistance (R_m) represents the loss in mechanical energy mainly dissipated to the surrounding medium and quartz interior. The change of motional resistance (ΔR_m) reflects the variation in the viscoelasticity of the film and in the viscosity and density of the contacting solution.

The typical PQCI response parameters (ΔR_m, Δf, ΔC_m, ΔL_m and ΔC_s) during mineralization of the HAP/CS composite in SBF solution are shown in Fig. 1(a). It can be seen that as Δf and ΔC_s decrease, ΔR_m increases, and ΔC_m and ΔL_m change modestly. The decrease of Δf is due to the mineralization of the HAP/CS composite in SBF solution; specifically Ca^{2+} and PO_4^{3-} ions are coupled electrostatically with carbonyl groups and amine groups of CS on the electrode surface, thus increasing the mass of the electrode surface film. In Fig. 1(b), the horizontal line for the initial 500 min exhibits the mass binding on the electrode surface(Marx et al., 2003). After mineralization, HAP crystals gradually grow on the surface of film, resulting in viscoelasticity change of the film, which brings ΔR_m increase and Δf decrease. The slip of Δf versus ΔR_m shows mass change and energy dissipation properties.

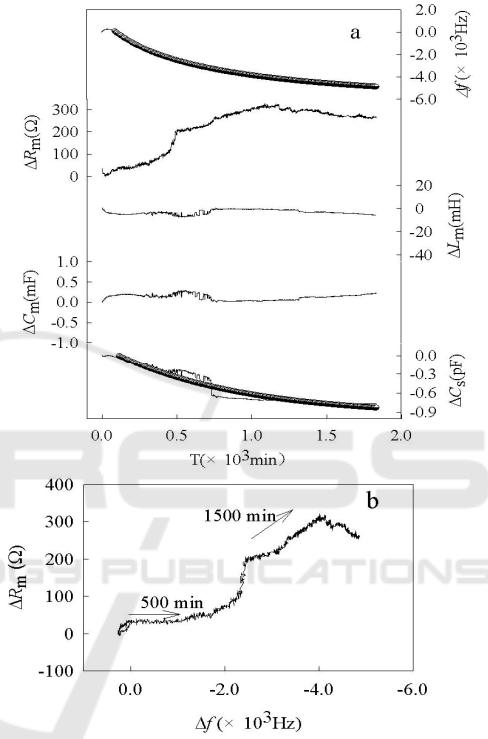

Fig. 1. (a)Time course of simultaneous responeses of ΔR_m, Δf, ΔC_m, ΔL_m and ΔC_s during the mineralization of the HAP/CS composite in SBF solution; (b) Δf vs. ΔR_m diagram for the mineralization of HAP/CS composite.

The static capacity, C_s is related to the capacity and structure of the electrical double layer at the charge interface. ΔC_s will provide the information on the capacity and structure of the interface. In this experiment, C_s decreases gradually; this may be caused by the mineralization of HAP/CS composite that results in thicker film. Furthermore, the deposited HAP covers the surface of HAP/CS composite resulting in hydrophilicity decrease and subsequent reduction in ion transfer. And, the dielectric constant of the film also varies with HAP formation. These factors combine to cause a decrease of ΔC_s.

The mineralization of HAP/CS composite in SBF solution fits the two consecutive reactions kinetic model. That is to say, the mineralization of HAP/CS composite could be divided into consecutive reaction steps. A conceptual model advances carbonyl groups and amino groups of CS as nucleation sites for HAP crystallization through binding oppositely charged ions, calcium ion and phosphate ion. Therefore, there is heterogenous nucleation and growth of nano-HAP on the surface of composite. Moreover, Ca^{2+} ions enrich the carbonyl groups and amino groups of CS in SBF solution and PO_4^{3-} enrich the amino groups of CS; this enrichment may be attributed to electrostatic interaction or/and polar interaction. Finally, heterogeneous nucleation of HAP on the surface of films forms crystals of HAP gradually. Due to OH^- and CO_3^{2-} doping in SBF solution, HAP crystalline grew and formatted a biological active bone-like carbonateapatite layer with mineralization times increasing. The process of HAP crystal growth is illustrated in Scheme 1.

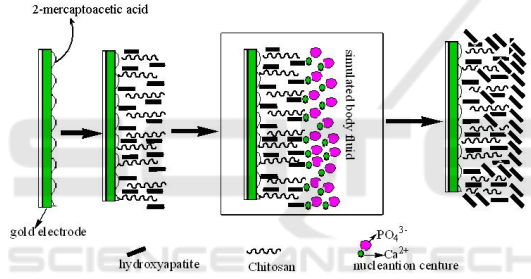

Scheme 1. Schematic process of different steps involved calcium phosphate crystals on HAP/CS composite.

3.2 SEM Characterization

Fig. 2 shows the SEM micrographs of HAP/CS at 12,000× after soaking in simulated body fluid for various periods. In Fig. 2(a), porous structure is observed before HAP/CS immersion. After mineralizing for 500 min, white granules are found in Fig. 2(b), which are HAP crystal consisting of numerous tiny flake. It is considered that a single layer of HAP particles start to deposit over the surface. This microstructure corresponds to the reported literature(Ramila et al., 2002; Zhu et al., 2007). Then, at time of 1500 min in Fig. 2(c), the surface is almost covered with calcium phosphate particles accompanied by a secondary nucleation over the initial layer. With increase of the immersion time, the crystal grains congregate together and form the porous HAP layer. Finally, the HAP crystal grains fill in the porous HAP layer and grow a dense structure in Fig. 2(d). Due to the HAP component of the starting material, the HAP induced the new nucleation and it grew vertically on the surface. This microstructure corresponds to that deposited on a bioactive glass or ceramics from SBF solution(Oliveira et al., 2009; Davidenko et al., 2010). To observe the typical HAP shape, it must be at higher magnifications. Oliveira et al. reported that it was possible a needle-like nanostructure for characteristic of Ca-P coatings formed under the present biomimetic conditions. Changes of morphology and structure of various stages demonstrate the nucleation and crystal growth.

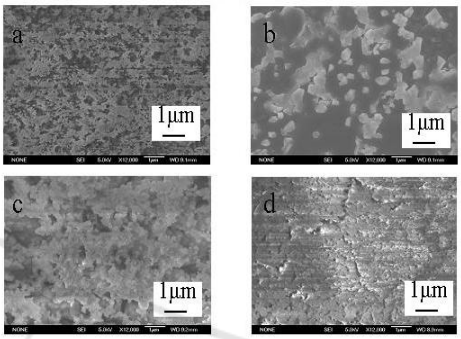

Fig. 2. SEM images (12,000×) of HA/CS after soaking in SBF solution at 0 min (a), 500 min (b), 1500 min (c), 2000 min (d).

3.3 Electrochemical Impedance Investigation and Cyclic Voltammetry Measurement

In order to clarify the difference among the mineralization films of the HAP/CS composite, electrochemical impedance spectroscopy and cyclic voltammetry were carried out before and after mineralization. Fig. 3 shows the electrochemical impedance spectroscopy and cyclic voltammetry for crystal modified with HAP/CS composite and the crystal immersion in SBF for 12 h and 24 h, respectively. The measurements were conducted in a phosphate buffer solution (pH=7.4) containing 0.2 M NaCl, 1mM $K_3[Fe(CN)_6]$ and 1mM $K_4[Fe(CN)_6]$. The semicircle region lying on the Z_{re} axis included in the electrochemical impedance spectroscopy corresponds to the electron transfer limited process, where the diameter corresponds to the electron transfer resistance (R_{et}) of the ferri-/ferrocyanide probe at the gold electrode interface. Fig. 3(a) illustrates that the electron-transfer resistance increases with the mineralization process in the SBF

solution. For the crystal modified with HAP/CS composite, the crystal after 12 h and 24 h of immersion in the SBF solution, mineralization introduces a barrier to interfacial electron transfer, corresponding to the interfacial electron transfer resistance Ret of about 323 Ω, 13300 Ω and 304700 Ω, respectively. This is mainly attributed to the mineralization of HAP/CS in SBF solution, which insulates the conductive support. As shown in the Fig. 3b, $K_3Fe(CN)_6$/K4Fe(CN)$_6$ shows the reversible behavior of HAP/CS coated electrode with a peak-to-peak separation ΔE_p of 105 mV and a reduction peak current I_p of 32 μA. Peak currents decreased sharply after HAP/CS composite was immerged into the SBF solution for 12 h, and peak currents are almost zero for 24 h. This is attributed to the film thickening for mineralization of HAP/CS, which results in the ferri-/ferrocyanide prode might be blocked to the bare electrode.

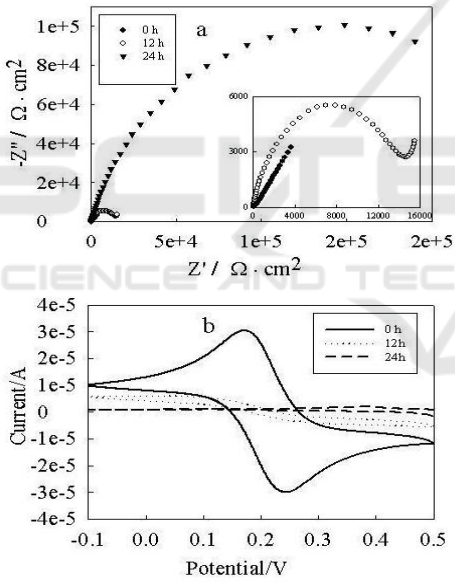

Fig. 3. Electrochemical impedance spectra (a) for crystal modified with HAP/CS composite, the crystal immersion in SBF for 12 h and 24 h as well as Cyclic voltammograms (b) for crystal modified with HAP/CS composite, the crystal immersion in SBF for 12 h and for 24 h in a PBS solution (pH 7.4) containing 0.2 M NaCl, 1mM $K_3Fe(CN)_6$ and 1mM $K_4Fe(CN)_6$. (a) 100 kHz~10 mHz, 10 mV rms, 0.17V versus SCE; (b) dE/dD=50 mV/s.

3.4 FT-IR Spectroscopy Characterization

In order to further characterize the mineralization of HAP/CS composite in the SBF solution, FT-IR spectrum analysis is performed and the spectra for mineralized material are shown in Fig. 4. The peaks at 1602 and 1484 cm^{-1} are due to the amide I carbonyl stretch of chitosan, which disappear gradually with mineralization of HAP/CS composite in the SBF solution. It is thought that there are chemical interactions between the amide of the chitosan and phosphates take place in the SBF solution. On the other hand, the FT-IR spectrum of three samples show that the typical peaks of phosphate stretching vibration occur at 1027-1180 cm^{-1}, and the peaks of bending vibrations of PO_4^{3-} group are observed at 630 and 525 cm^{-1}. Furthermore, the adsorption peak displays greater strength and acuity when the HAP/CS composite is immerged in SBF solution for 24 h indicating formation of crystal HAP with the mineralization. Peaks for CO_3^{2-} vibration mode appear at positions 740, 840, and 1458-1472 cm^{-1} indicating that HAP crystals are formed on the surface of composite films; meanwhile, the PO_4^{3-} sites of the nano-HAP are partly substituted by CO_3^{2-} groups. One may deduce that there is formation of crystallized carbonateapatite during mineralization of the /CS composite in the SBF solution, which suggests that the bioactivity of the HAP/CS composite can form a biological active bone-like, carbonateapatite.

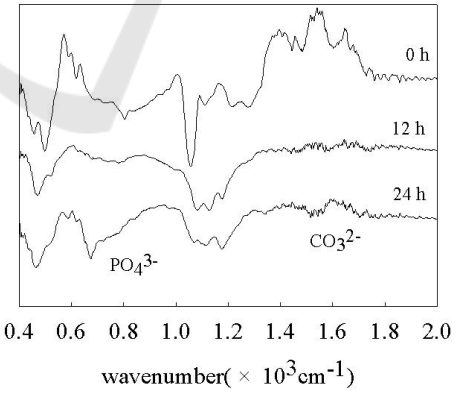

4. FT-IR spectrum of HAP/CS composite mineralized at different time.

3.5 XRD Analysis

The XRD patterns of the HAP/CS after mineralization in SBF and pure CS are shown in Fig.

5. The XRD pattern of pure CS showed two typical peaks at 2θ = 11° and 20°, which corresponds to the reported literature(Samuels 2010). After mineralization in SBF solution, the HAP/CS composite showed the characteristic peaks (26° and 32°) of hydroxyapatite, similar to that reported by Kong et al(Kong et al., 2006). As the HAP peaks are comparatively broader than a normal HAP specimen, it is considered that the HAP crystals were small crystallite size. Combined with the results of FT-IR, it can be deduced that the induced apatite was a carbonate HAP.

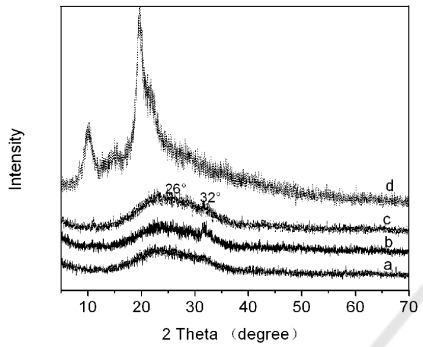

Fig. 5 X-ray diffraction patterns of HAP/CS composite material mineralized at (a)500min, (b)1500min, (c)2000min and (d)pure CS.

4 CONCLUSIONS

The mineralization kinetics of HAP/CS composite were investigated by the piezoelectric quartz crystal impedance combining with electrochemical impedance spectroscopy and cyclic voltammetry, the dynamically structural and morphological characterization of mineralization products on various stages by SEM, FT-IR and XRD. The changes of PQCI parameters demonstrate the changes of the physical and chemical properties between the interfaces of the HAP/CS composite and the SBF solution. Two parameters, Δf and ΔC_s, were used to simultaneously estimate the mineralization process of HAP/CS composite in SBF solution. Its process is comprised of nucleation and growth of crystal of HAP, and their kinetics and mechanism are analyzed. The results demonstrate the validity of the proposed method for its ability to provide real time multidimensional information during the mineralization process; therefore the present method will play an important role for investigating biomaterial mineralization.

ACKNOWLEDGEMENTS

The present study was supported by Hunan Provincial Natural Science Foundation of China (2015JJ6025) and the Doctoral Scientific Fund Project of Hunan Institute of Engineering (2014086).

REFERENCES

1. Moore, R., Lopes, J., 1999. Paper templates. In *TEMPLATE'06, 1st International Conference on Template Production*. SCITEPRESS.
2. Smith, J., 1998. *The book*, The publishing company. London, 2nd edition.
3. Baker K., Anderson M., Oehlke S., Astashkina A., 2006, Growth, characterization and biocompatibility of bone-like calcium phosphate layers biomimetically deposited on metallic substrata, Materials Science Engineering C 26,1351-1360.
4. Shadanbaz S., Dias C., 2012, Calcium phosphate coatings on magnesium alloys for biomedical applications: a review, Acta Biomaterials 8,20-30
5. chen F., Zhu Y., 2014, Multifunctional calcium phosphate nanostructured materials and biomedical applications, Current Nanoscience 10,465-485
6. Liu B., Zhang X., Xiao G., Lu Y., 2015, Phosphate chemical conversion coatings on metallic substrates for biomedical application: A review, Materials Science and Engineering C 47,97-104
7. Cengiz B., Gokce Y., Yildiz N., Aktas Z., Calimli A., 2008,Synthesis and characterization of hydroxyapatite nanoparticles, Colloids Surface A 322,9-25.
8. Balasundaram G., Sato M., Webster T., 2006, Using hydroxyapatite nanoparticles and decreased crystallinity to promote osteoblast adhesion similar to functionalizing with RGD, Biomaterials 27,2798-2805.
9. Wang H., Li Y., Zuo Y., Li J., Ma S., Cheng L., 2007, Biocompatibility and ostegenesis of biomimetic nano-hydroxyapatite/polyamide composite scaffolds for bone tissue engineering, Biomaterials 28,3338-3348.
10. Petro I., Kalinkevich O., Pogorielov Ma., Kalinkevich A., Stanislavov A., et al., 2016, Dielectric and electric properties of new chitosan-hydroxyapatite materials for biomedical application: Dielectric spectroscopy and corona treatment, Carbohydrate polymers 151,770-778
11. Pangon A., Saesoo S., Saengkrit N., Ruktanonchai U., Intasanta V., 2016, Hydroxyapatite-hybridized chitosan/chitin whisker bionanocomposite fibers for bone tissue engineering applications, Carbohydrate Polymers 144, 419-427.
12. Zhao Y., Jiang Z., Xiao L., Xu T., Qiao S., Wu H., 2011,Chitosan membranes filled with biomimetic

mineralized hydroxyapatite for enhanced proton conductivity, Solid State Ionic. 187,33-38
13. Jiang L., Li Y., Wang X., Zhang L., Wen J., Gong M., 2008, Preparation and properties of nano-hydroxyapatite/chitosan/carboxymethyl cellulose composite scaffold, Carbohydr Polym 74,680-684.
14. Zhang J., Liu G., Wu Q, Zuo J., Qin Y., Wang J.,2012, Novel mesoporous hydroxyapatite/chitosan composite for bone repair, Journal of Bionic Engineering 9,243-251 .
15. Bayrak G., Demirtaş T., Gümüşderelioğlu D., 2017,Microwave-induced biomimetric approach for hydroxyapatite coatings of chitosan scaffolds, Carbohydrate Polymers. 157,803-813
16. Lei Y., Xu Z., Ke Q., Yin W., Chen Y., Zhang C., Guo Y.,2017, Strontium hydroxyapatite/chitosan nanohybrid scaffolds with enhanced osteoinductivity for bone tissue engineering, Materials Science and Engineering C 72,134-142.
17. Ohtsuki C., Kamitahara M., Miyazaki T.,2007, Coating bone-like apatite onto organic substrates using solutions mimicking body fuild, Journal of Tissue Engineering Regenerative Medicine. 1,33-38
18. Shahriarpanah S., Nourmohammadi J., Amoabediny G., 2016, Fabrication and characterization of carboxylated starch-chitosan bioactive scaffold for bone regeneration, International Journal of Biological Macromolecules. 93,1069-1078
19. Li J., Zhu D., Yin J., Liu Y., Yao F., Yao K., 2010, Formation of nano-hydroxyapatite crystal in situ in chitosan-pectin polyelectrolyte complex network, Materials Science and Engineering C 30, 795-803
20. Manjubala I., Scheler S., Bossert J., Jandt K., 2006, Mineralisation of chitosan scaffolds with nano-apatite formation by double diffusion technique, Acta Biomaterials 2,75-84.
21. Meng D., Dong L., Wen Y., Xie Q., 2015, Effects of adding resorbable chitosan microspheres to calcium phosphate cements for bone regeneration, Materials Science and Engineering C 47,266-272
22. Kong L., Gao Y., Lu G., Gong Y., Zhao N., Zhang X., 2006, A study on the bioactivity of chitosan/nano-hydroxyapaptite composite scaffolds for bone tissue engineering, European Polymer Journal 42,3171-3179.
23. Yin N., Chen S., Yang Y., Tang L., Yang J., Wang H., 2011, Biomimetic mineralization synthesis of hydroxyapatite bacterial cellulose nanocomposites, Progress in Natural Science: Materials International 21,472-477
24. Barrere F., Blitterswijk C., Groot K., Layrolle P., 2002, Influence of ionic strength and carbonate on the Ca-P coating formation from SBF×5 solution, Biomaterials 23,1921-1940.
25. Muramatsu H., Suda M., Ataka T., Seki A., Tamiya E., karube I., 1990, Piezoelectric resonator as a chemical and biochemical sensing device, Sensors Actuators A Physical 21,362-368.
26. Muramatsu H., Tamiya E., Suzuki M., Karube I., 1988, Viscosity monitoring with a piezoelectric quartz crystal and its application to determination of endotoxin by gelation of limulus amebocyte lysate, Analytical Chimica Acta 215,91-99.
27. Sauerbrey G., 1959, The use of quartz oscillators for weighting thin layers and for microweighing, Z. Physical 155,206-222.
28. Wang Q.L., Ge S., Zhu H., 2004, Studies on the synthesis and structure of nanosized hydroxyapatite crystals at normal temperature and atmospheric press, China University Mining Technology 33,533-536. (in chinese).
29. Xu C., He D., Zeng L., Luo S., 2009, Biomineralization of hydroxyapatite-chitosan composite in a simulated body fluid using piezoelectric quartz crystal impedance, Journal of Central South University (Science and Technology) 40,334-339. (in chinese)
30. Muramatsu H., Tamiya E., Karube I., 1988, Computation of equivalent circuit parameters of quartz crystals in contact with liquids and study of liquid properties, Analytical Chemistry 60,2142–2146.
31. Marx K., 2003, Quartz crystal microbalance: A useful tool for studying thin polymer films and complex biomolecular systems at the solution-surface interface, Biomacromolecules 4,1099-1120.
32. Rámila A., Padilla S., Muñoz B., Vallet-Regí M., 2002, A new hydroxyapatite/glass biphasic Material: In vitro bioactivity, Chemistry Materials 14, 2439-2433.
33. Zhu Z., Tong H., Jiang T., Shen X., Wan P., Hu J., 2006, Studies on induction of L-aspartic acid modified chitosan to crystal growth of the calcium phosphate in supersaturated calcification solution by quartz crystal microbalance, Biosensors Bioelectronics 22,291-297.
34. Oliveira A., Costa S., Sousa R., Reis R., 2009, Nucleation and growth of biominetic apatite layers on 3D plotted biodegradable polymeric scaffolds: Effect of static and dynamic coating conditions, Acta Biomaterialia 5, 1626-1638.
35. Davidenko N., Carrodeguas R., Peniche C., Solís Y., Cameron R, 2010, Chitosan/apatite composite beads prepared by in situ generation of apatite or Si-apatite nanocrystals, Acta Biomaterialia 6, 466-14.
36. Samuels R., 1981, Solid state characterization of the structure of chitosan film, Journal Polymer Science: Polymer Physics Edition 19,1081-1105.